Complex Patterning by Vertical Interchange Atom Manipulation Using Atomic Force Microscopy

plitude stability of the PSWS experiment. Such studies could help to promote a fundamental understanding of spin-polarized transport in various itinerant ferromagnets, in that spin waves provide both a well-defined inhomogeneous magnetization configuration for performing spin transfer and an accurate probe with which to measure it.

References and Notes

1. J. C. Slonczewski, *J. Magn. Magn. Mater.* **159**, L1 (1996).
2. L. Berger, *Phys. Rev. B* **54**, 9353 (1996).
3. E. B. Myers, D. C. Ralph, J. A. Katine, R. N. Louie, R. A. Buhrman, *Science* **285**, 867 (1999).
4. M. D. Stiles, J. Miltat, in *Spin Dynamics in Confined Magnetic Structures* (Springer, New York, 2006), vol. 3, pp. 225–308.
5. M. Tsoi *et al.*, *Nature* **406**, 46 (2000).
6. W. H. Rippard, M. R. Pufall, in *Handbook of Magnetism and Advanced Magnetic Materials*, H. Kronmüller, S. Parkin, Eds (Wiley, New York, 2007), vol. 2, pp. 1167–1191.
7. A. Yamaguchi *et al.*, *Phys. Rev. Lett.* **92**, 077205 (2004).
8. L. Thomas, S. Parkin, in *Handbook of Magnetism and Advanced Magnetic Materials*, H. Kronmüller, S. Parkin, Eds (Wiley, New York, 2007), vol. 2, pp. 942–982.
9. Y. B. Bazaliy, B. A. Jones, S. C. Zhang, *Phys. Rev. B* **57**, R3213 (1998).
10. J. Fernández-Rossier, M. Braun, A. S. Nuñez, A. H. MacDonald, *Phys. Rev. B* **69**, 174412 (2004).
11. L. L. Hirst, *Phys. Rev.* **141**, 503 (1966).
12. S. Zhang, Z. Li, *Phys. Rev. Lett.* **93**, 127204 (2004).
13. A. Thiaville, Y. Nakatani, J. Miltat, Y. Suzuki, *Europhys. Lett.* **69**, 990 (2005).
14. J. Xiao, A. Zangwill, M. D. Stiles, *Phys. Rev. B* **73**, 054428 (2006).
15. Materials and Methods are available as supporting material on *Science* Online.
16. T. P. Gill, *The Doppler Effect, An Introduction to the Theory of the Effect* (Logos Press, London, 1965).
17. D. D. Stancil, B. E. Henty, A. G. Cepni, J. P. Van't Hof, *Phys. Rev. B* **74**, 060404 (2006).
18. P. Lederer, D. L. Mills, *Phys. Rev.* **148**, 542 (1966).
19. A. G. Gurevich, G. A. Melkov, *Magnetization Oscillations and Waves* (CRC Press, 1996).
20. D. D. Stancil, *Theory of Magnetostatic Waves* (Springer, New York, 1993).
21. M. Bailleul, D. Olligs, C. Fermon, *Appl. Phys. Lett.* **83**, 972 (2003).
22. H. Hurdequint, *J. Magn. Magn. Mater.* **242–245**, 521 (2002).
23. J. Bass, W. P. Pratt Jr., *J. Magn. Magn. Mater.* **200**, 274 (1999).
24. I. A. Campbell, A. Fert, in *Ferromagnetic Materials*, E. P. Wohlfarth, Ed. (North-Holland, Amsterdam, 1982), vol. 3, pp. 747–804.
25. P. E. Mijnarends, S. Sahrakorpi, M. Lindroos, A. Bansil, *Phys. Rev. B* **65**, 075106 (2002).
26. J. Banhart, H. Ebert, A. Vernes, *Phys. Rev. B* **56**, 10165 (1997).
27. A. F. Mayadas, J. F. Janak, A. Gangulee., *J. Appl. Phys.* **45**, 2780 (1974).
28. G. S. D. Beach, C. Knutson, C. Nistor, M. Tsoi, J. L. Erskine, *Phys. Rev. Lett.* **97**, 057203 (2006).
29. We thank J. Grollier and C. Deranlot (UMR CNRS/Thalès) for providing the permalloy films, H. Hurdequint for advice, A. Carvalho for assistance with e-beam lithography, A. Boulard for the fabrication of the measurement set-up, and K. Hajjia for measurements on unprocessed films. Support from the staff of the Consortium de Nanosciences et de Nanotechnologies de Strasbourg nanofabrication facilities and financial support from Agence Nationale de la Recherche "spectrospin" and from Region Alsace are gratefully acknowledged.

Complex Patterning by Vertical Interchange Atom Manipulation Using Atomic Force Microscopy

Yoshiaki Sugimoto,[1] Pablo Pou,[2] Oscar Custance,[3]* Pavel Jelinek,[4] Masayuki Abe,[1,5] Ruben Perez,[2] Seizo Morita[1]

The ability to incorporate individual atoms in a surface following predetermined arrangements may bring future atom-based technological enterprises closer to reality. Here, we report the assembling of complex atomic patterns at room temperature by the vertical interchange of atoms between the tip apex of an atomic force microscope and a semiconductor surface. At variance with previous methods, these manipulations were produced by exploring the repulsive part of the short-range chemical interaction between the closest tip-surface atoms. By using first-principles calculations, we clarified the basic mechanisms behind the vertical interchange of atoms, characterizing the key atomistic processes involved and estimating the magnitude of the energy barriers between the relevant atomic configurations that leads to these manipulations.

Scanning tunneling microscopy (STM) has proven to be the method of excellence for creating nanostructures on surfaces, manipulating atoms and molecules one at a time (*1–3*). A new panorama has recently been opened by the capability of atomic force microscopy (AFM) to create similar nanostructures atom by atom (*4*) and to quantify the forces involved in these lateral manipulations (*5, 6*).

When exploring a surface with these scanning probe methods, the apex of the probe can be contaminated with atomic species present at the surface (*7*) by picking up atoms in accidental or intended mechanical contacts with the surface. Advantage could be taken of this situation, and an atomic version of the dip-pen nanolithography (*8*) may be implemented: Atoms wetting the tip apex could be individually deposited to write patterns at heterogeneous surfaces. We provide evidence that such an atomic pen can be implemented by using AFM.

We performed the AFM experiments (*9*) in dynamic mode under the frequency modulation detection scheme (*10*), keeping the cantilever oscillation amplitude constant. Commercial silicon cantilevers, which have very sharp tips at their free ends, were used to image the Sn/Si(111) − ($\sqrt{3} \times \sqrt{3}$)R30° surface (*11*) by detecting the short-range chemical interaction force between the closest tip and surface atoms (*9*).

The inset of Fig. 1A shows topographic images of a single atomic layer of tin (Sn) atoms, which appear as bright protrusions, grown over a silicon (111) single-crystal substrate. Among the atomic defects this surface exhibits (*11*), the most representative ones are substitutional silicon (Si) atoms (*12*) at the perfect Sn atomic layer, and these appear as protrusions with diminished contrast. We have observed that these Si defects can be vertically manipulated during force spectroscopy (*13, 14*) experiments. After imaging the surface and positioning the AFM tip with a lateral precision better than ±0.1 Å (*15*) over the topmost part of the marked Si atom, we moved the sample toward the oscillating AFM probe. At a given tip-surface distance, an instability in the frequency shift occurs, as highlighted by the arrow in the graph. In an image taken after the sample was retracted, the Si atom was no longer visible, and a Sn atom was found to occupy the corresponding lattice position instead (Fig. 1A, bottom right inset). One hypothesis to explain this event is that the Si atom at the surface has been replaced by a Sn atom originally located at the tip apex, as sketched out by the illustration in Fig. 1A. The same procedure can be consecutively applied to the freshly deposited Sn atom (marked with a circle in Fig. 1B, left inset), resulting in the replacement of this surface atom by a Si atom coming from the tip and in a partial loss of atomic contrast (Fig. 1B, bottom right inset). Because all the images shown in Fig. 1 were acquired under the same experimental parameters,

[1]Graduate School of Engineering, Osaka University, 2-1 Yamada-Oka, 565-0871 Suita, Osaka, Japan. [2]Departamento de Física Teórica de la Materia Condensada, Universidad Autónoma de Madrid, 28049 Madrid, Spain. [3]National Institute for Materials Science, 1-2-1 Sengen, 305-0047 Tsukuba, Ibaraki, Japan. [4]Institute of Physics, Academy of Sciences of the Czech Republic, Cukrovarnicka 10, 1862 53 Prague, Czech Republic. [5]Precursory Research for Embryonic Science and Technology, Japan Science and Technology Agency (JST), 332-0012 Saitama, Japan.

*To whom correspondence should be addressed. E-mail: custance.oscar@nims.go.jp

this contrast change should correspond to a modification of the tip apex (fig. S4) (9). This tip modification is, however, not irreversible. By scanning aside a region that neighbors the imaged area at vertical distances slightly closer to the surface than that used for imaging, we recovered good atomic contrast again for most of the test performed (fig. S1) and were able to repeat these manipulation processes multiple times (fig. S2). Dissipation signals (16) of up to 1.2 eV per cycle accompanied these atomic interchanges between the tip and surface (fig. S1). Although the vertical manipulations described here were performed at room temperature, they have also been accomplished at low temperature (80 K).

This vertical interchange of strongly bound atoms between the tip and the surface differs from methods previously reported using STM, in which an atom weakly bonded on a metallic surface can be reversibly transferred between the tip and the surface by applying an appropriate bias voltage (17). It also diverges from other methods of controlled atom manipulations recently achieved with AFM (4–6) that make use of the attractive part of the tip-surface interaction to laterally manipulate atoms without any active participation of the tip, which is only used to tune the interaction of the manipulated atom with the surface. In contrast, the mechanism of the manipulations reported here is based on a process in which the vertical interchange of atoms is controlled by the mechanical properties of a hybrid tip-surface structure formed in the repulsive regime of the tip-surface interaction force.

Although imaging and manipulation in the attractive regime involve mainly the bonding interaction between the closest tip-surface atoms, in the repulsive regime a larger contact involving several atoms is expected, leading to a very complex energy landscape. The structure of the contact at the closest approach determines the most likely outcome among the different competing processes: atom interchange, atom trans-

fer to the tip, or deposition of tip atoms when the tip is pulled out from the surface. However, the reproducibility of the vertical atomic interchange and the resemblance of recorded frequency shift and force curves in experiments performed with different tips (figs. S1 and S2) point toward a common basic microscopic mechanism.

To characterize the atomistic processes, we performed simulations of the tip-surface approach and retraction events. These simulations (9) are based on density functional theory first-principles calculations implemented with a local orbital basis using the FIREBALL code (18). To model the experimental tip apex, we considered a rigid tip (Fig. 2B) on which only the two atoms in the dimer defining the apex were allowed to relax upon interaction with the surface. We imposed this constraint on the tip model in order to simplify the complex configuration space associated with the tip mechanical response.

Figure 2A illustrates, using the total energy, the evolution of the system during an alternate deposition of a Sn atom (solid lines) and Si atom (dashed lines); the most relevant atomic configurations during both processes are depicted in Fig. 2B. For the Sn deposition, the system follows branch A (squares), starting at A_1, where there is no substantial interaction, and enters the attractive regime as the tip approaches the surface. At A_2, the system is near the total energy minima, and further tip-surface approach leads to a repulsive force that increases up to structure A_3, in which the atoms are considerably compressed but still keep their original bonding topology. Upon retraction from any tip-surface distance larger than the one corresponding to A_3, the system follows the same energy curve back to the original structure A_1. Approaching the tip beyond A_3, the system undergoes a discontinuous jump to a new energy branch B (triangles) with a substantially different bonding topology (Fig. 2B, image B_1). During further approach and consecutive retraction, the system follows this energy branch up to B_2, where a jump takes it to another energy solution [branch C (circles)], lead-

ing to the bonding topology (structure C_2) and the atomic interchange. The Si deposition case presents the same basic features. During approach, the system follows the C branch until reaching C_3, where it jumps to branch D (pentagons). Retraction from any distance along the D branch after this jump leads to a new jump from D_2 to A_2 and to the atom interchange. Comparing the two deposition cases, although the atomistic details are slightly different, overall the atom interchange mechanism seems to be the same. The key step in these processes is to reach the dimer-like structure shown in B_1 and D_1. In these atomic configurations, the outermost atom of the tip and the atom at the surface now have an equal number of bonds with the surrounding atoms, losing their association as being part of the tip or the surface. Our simulations confirm that the dimer structure that minimizes the stored elastic energy under compression is the lowest energy configuration for other tip-surface orientations and even for different tip structures.

The energy landscape of these atomic interactions sheds light on some of the features observed in the associated experimental curves. The frequency shift signals (Fig. 1) display a shoulder at closer tip-surface distances that develops into a double well structure in the corresponding short-range chemical interaction forces (figs. S1 and S2), in contrast to canonical force spectroscopy curves that for this system can be found in figures 3 and 5 of (12). The presence of several possible pathways in either a Sn or a Si deposition manifests in different solutions of the tip-surface interaction force. However, because the frequency shift is proportional to a weighted average of the tip-surface interaction force over one oscillation cycle (19, 20), the existence of these pathways is blurred (16) in the frequency shift and thus in the short-range chemical interaction force derived from it. Both the frequency shift and the obtained interaction force should not a priori bear information about nonconservative tip-surface interactions (19, 21, 22) that lead to a dissipation of energy from the

Fig. 1. Alternate vertical interchange atom manipulations. (**A**) Frequency shift (Δf) signal upon approach (black) and retraction (red) of the tip over the Si atom marked with a white circle in the left inset image. In a consecutive topographic image to the curve acquisition (bottom right inset), a Sn atom appears at the same surface location instead. The Si atom was replaced by a Sn atom coming from the tip (Sn deposition). (**B**) Frequency shift signal upon approach (black) and retraction (red) of the tip above the Sn atom deposited in (A), pointed out by a black circle (left inset). After the curve acquisition, the replacement of this Sn atom by a Si atom coming from the tip (Si deposition) and a partial loss of atomic contrast are obtained (bottom right inset). For comparison with other curves, the normalized frequency shift (γ) (19) is displayed in the vertical axis on the right. The black arrows in the plots indicate instabilities representative of the corresponding concerted vertical interchange of atoms between the tip and surface. The origin of the horizontal axes denotes the point of maximum proximity between
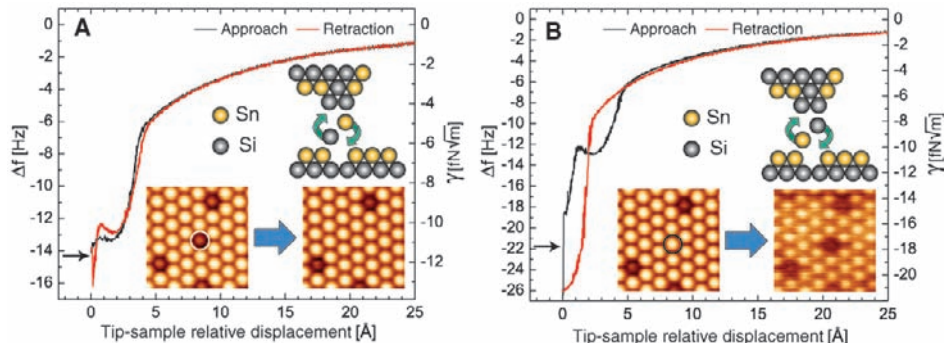
the tip and sample; this criterion was adopted for all the experimental curves shown in this work. The illustrations are representations of the corresponding vertical atomic interchange, with yellow and gray spheres symbolizing Sn and Si atoms, respectively; they do not bear any realistic information about the tip-apex structure or composition. For the acquisition parameters and analysis of the short-range forces associated with these manipulations, see fig. S1.

cantilever oscillation (*16*, *23*, *24*). The energy barriers between branches as a function of the tip-surface distance dictate where the system jumps during either approach or retraction and thus determine the details of both frequency shift and force curves (fig. S3) (*9*). The shoulder in the frequency shift curves, the double-well structure in the short-range chemical forces, and the energy dissipation indicate that the system is evolving between two different bonding configurations during an approach-and-retraction cycle. These configurations must be stable enough to be reproduced over multiple approach-and-retraction cycles of the oscillating tip at the closest tip-surface distances.

These vertical interchange atomic manipulations require a tip rigid enough to endure high loads over the repulsive part of the short-range chemical interaction without undergoing major structural modifications, which is the norm under these conditions. We have found tips that can alternatively deposit Sn and Si atoms (Fig. 1 and fig. S2), others that can just deposit Sn atoms (fig. S5) (*9*), and some tips that only deposit Si atoms. We have not been able to develop a systematic way of producing such tips yet, and success in identifying them relies on making a number of gentle tip-surface contacts using the same cantilever over different measurement sessions. From our extensive force spectroscopy experiments on this surface (*14*), we have found that 29% of the tips produced vertical inter-

change atom manipulation, being almost equally probable to find tips producing either Si deposition or alternate deposition of Sn and Si atoms and less probable to have a tip depositing only Sn atoms. Once an atom exchanging tip is found, it is possible to perform the manipulations in a reproducible way. Figure 3 illustrates an example of the creation of complex atomic patterns by successively depositing individual Si atoms coming from the tip in processes similar to the one shown in Fig. 1B. The tip used to create these atomic patterns was only able to deposit Si atoms (Figs. 3B to 3M). Thus, to put aside the Si defect beside the "i" character in Fig. 3M, several in-plane lateral interchange manipulation steps performed as described in (*4*) (fig. S7) were successively applied. In contrast to previous atomic assemblies based on lateral atom manipulation with AFM (*4*), this vertical manipulation method reduces by almost a factor of 10 the time needed to create similar atomic patterns: it took us only 1.5 hours of mostly imaging time to build the structures shown in Fig. 3.

The creation of these atomic patterns must involve not only the repeated interchange of atoms between the tip and surface but also diffusion and segregation processes at the tip apex to guarantee the presence of the required chemical species in the appropriate atomic arrangement. The simulation of the whole process is far beyond the capabilities of current first-principles methods, yet insights into the influence of the tip mechanical

response can be gained just by approaching our initial tip model with a more realistic situation. To this end, we have allowed the four outermost atoms of the tip apex to relax. This option considerably enlarges the configuration space with processes including tip modifications and extraction of atoms from the surface (fig. S6) (*9*) that lead the system to a final state of energy higher than that for the vertical atomic interchange. Although at room temperature thermodynamics would favor the lowest energy final configurations, the feasibility of the process is controlled by the energy barriers among the different local minima. Figure 4A depicts the energy for an approach (squares) and retraction (triangles) cycle over a Si atom resulting in a tip change, in which the Sn atom at the apex is deposited over the surface atoms. Upon retraction, the system crosses an energy branch (circles) that corresponds to a tip retraction in which the surface Si atom is located at the dimer structure forming the tip apex and the tip Sn atom is now at the surface in a vertical atomic interchange similar to the one shown in Fig. 1A. Using the nudge elastic band method (*25*), we studied the transition between two atomic configurations very close in energy (points α and β) belonging to these two different energy solutions: The starting atomic arrangement (α) is a dimer-like configuration in which both atoms have lost their association as being part of the tip or the surface; the final state (β) is the deposition of the Sn atom. We found that

Fig. 2. First-principles simulations of vertical interchange atom manipulation processes. (**A**) Evolution of the total energy upon two consecutive approach-and-retraction cycles using a model rigid tip (only the two atoms in the dimer defining the apex are allowed to relax) over the same location of a Sn/Si(111) − ($\sqrt{3} \times \sqrt{3}$)R30° surface, which results in the alternate deposition of a Sn atom [first cycle (continuous lines)] and a Si atom [second cycle (dashed lines)], respectively. Upon increasing the load of the tip apex over the surface and consecutive retraction, atoms at both the tip and surface undergo a series of structural relaxations that manifest in jumps between different solutions that correspond to local energy minima. (**B** and **C**) Atomic configurations associated with the transitions between energy branches labeled in (A) showing the most relevant atomistic details involved in the concerted vertical interchange of atoms between the tip and surface. A detail of the bonding configuration evolution within the dashed line rectangles displayed in A$_2$ and C$_2$ of (B) is shown in (C).
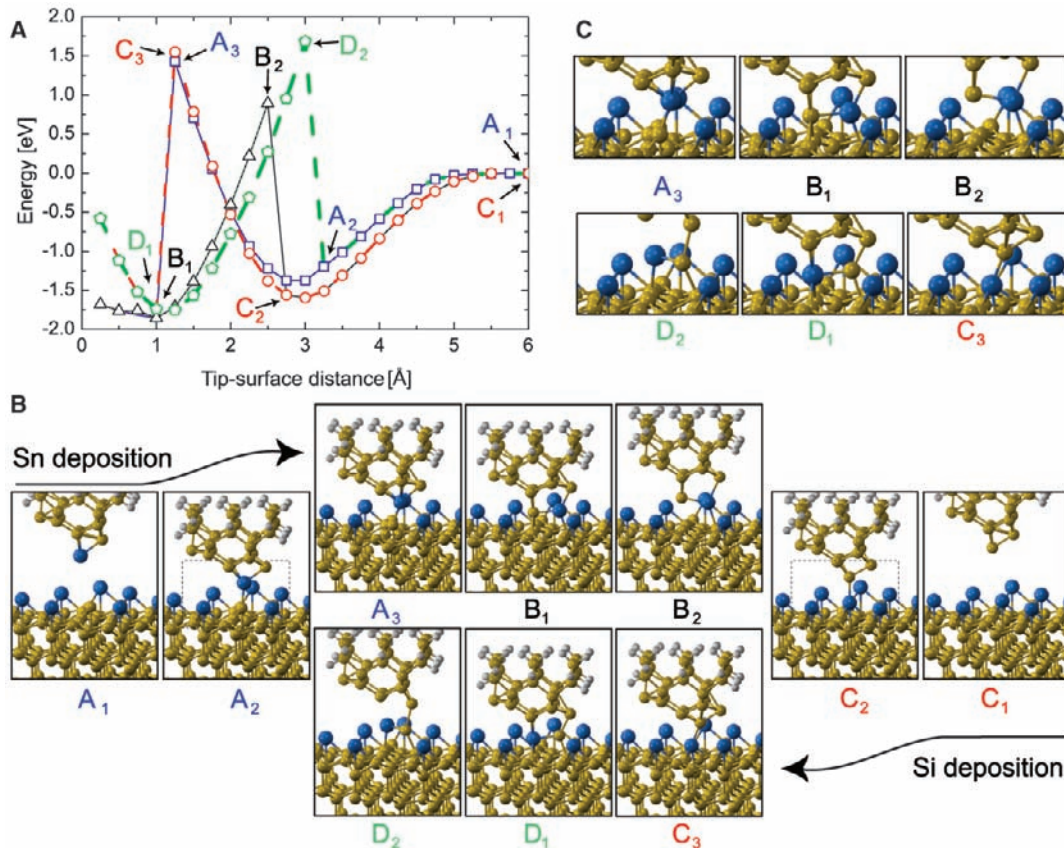
Fig. 3. Complex atomic patterning by vertical interchange atom manipulation at room temperature. (**A**) Illustration denoting the concerted vertical interchange of atoms between the tip and surface. (**B** to **M**) Series of topographic images showing the creation of atomic patterns displaying the symbol of silicon. These patterns were constructed by the successive substitution of Sn atoms at the surface one atom at a time with Si atoms coming from the tip. (**N**) Illustration denoting the concerted lateral interchange of surface atoms. (**O**) The Si atom adjacent to the "i" character in (M) was relocated to a nearby position in several in-plane lateral interchange atom-manipulation (*4*) events similar to the one depicted in fig. S7 (*9*). Acquisition parameters were a cantilever first mechanical resonant frequency of 193744.2 Hz, cantilever oscillation amplitude of 226 Å, and cantilever static stiffness of 48.8 N/m, with imaging Δf set point values between −5.5 Hz and −6.6 Hz.
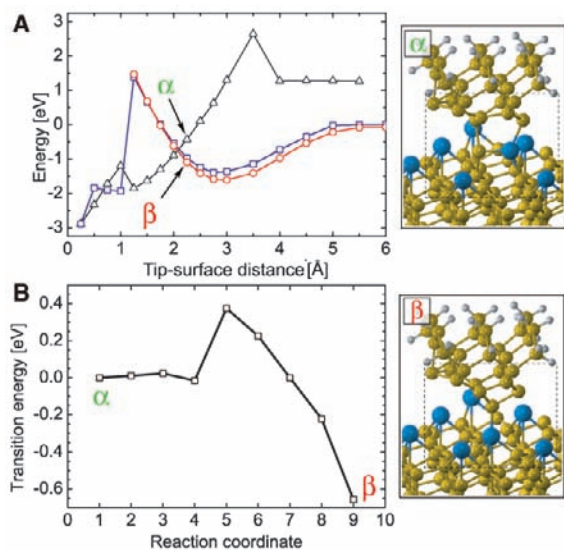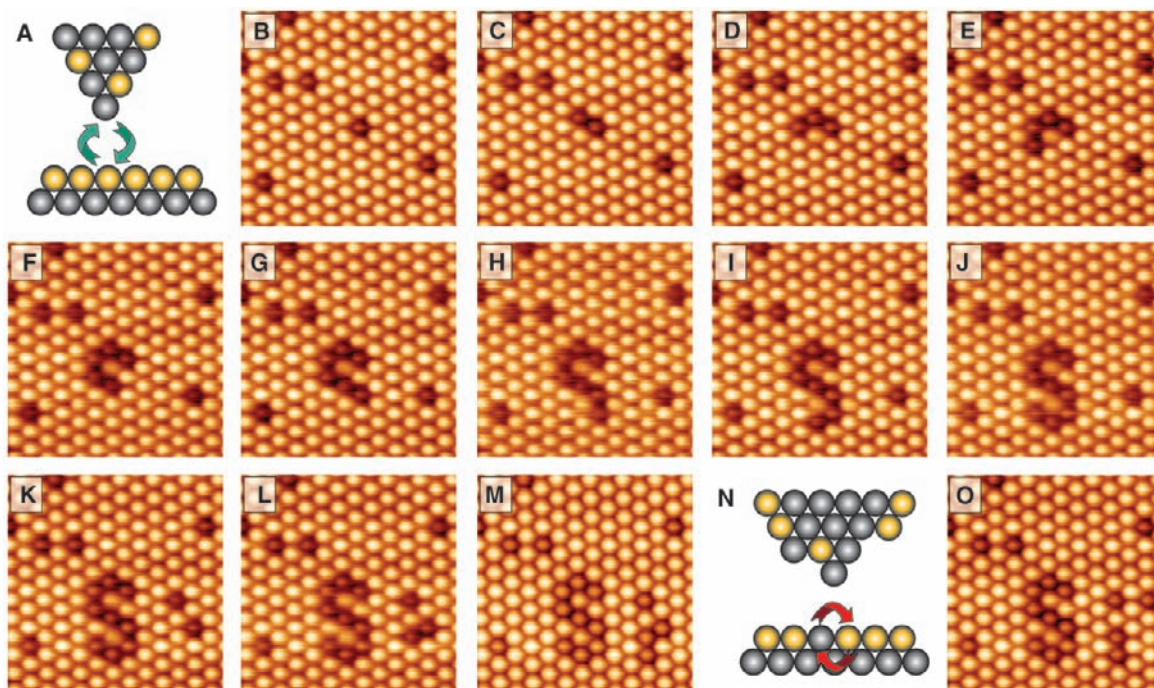
Fig. 4. Typical energy barriers involved in the concerted vertical interchange of atoms between the tip and surface. (**A**) Total energy solutions (squares and triangles) for a tip-surface approach-and-retraction cycle over a Si atom producing a tip modification in which the Sn atom at the apex is lost and left on the surface. The energy solution upon retraction (triangles) crosses an energy branch (circles) that would result in the concerted vertical interchange of these atoms. (**B**) Transition energy between two atomic configurations close in total energy labeled as α and β in (A). Energy barriers of a magnitude similar to the one shown in (B) can be easily overcome by atomic thermal fluctuations at room temperature. The atomic configurations corresponding to the points marked in (A) and (B) are displayed on the right. (**C**) Details of the bonding configurations, reaction coordinate (*9*) in (B), through the minimum energy path for the transition from state α to state β. The area displayed matches the dashed-line rectangles shown on the images on the right.

there is an energy barrier of 0.4 eV for the transition between these two configurations (Fig. 4B), which corresponds to the breaking of the remaining bond of the Si atom with the surface and the formation of a second bond of the Sn atom with the surface (Fig. 4C, images 4 to 6). This relatively small energy barrier does not prevent the process from taking place at room temperature, accounting as well for the presence of a considerable dissipation signal (fig. S1) at the closest tip-surface distances (*16, 23, 24*). Therefore, in the experiments it is not necessary to reach the high loads predicted in Fig. 2 for the atomic interchange taking place; just by exploring tip-surface distances close to the location of the repulsive zero short-range force (near the crossing point of the different energy branches available for the system), we are very likely to obtain a thermally activated vertical interchange atom manipulation.

The results reported here provide evidence that AFM can be used for the controlled deposition of individual atoms in semiconductor surfaces with the possibility of patterning complex atomic structures. Although our results focus on the Sn/Si system, we have found these vertical interchange atomic manipulations in other semiconductor surfaces (fig. S8). This manipulation technique may pave the way toward selective semiconductor doping (*26*), practical implementation of quantum computing (*27*), or atomic-based spintronics (*28*). The possibility of combining sophisticated vertical and lateral atom manipulations (*4, 6*) with the capability of AFM for single-atom chemical identification (*14*) may bring closer the advent of future atomic-level applications, even at room temperature.

References and Notes

1. D. M. Eigler, E. K. Schweizer, *Nature* **344**, 524 (1990).
2. M. F. Crommie, C. P. Lutz, D. M. Eigler, *Science* **262**, 218 (1993).

3. A. J. Heinrich, C. P. Lutz, J. A. Gupta, D. M. Eigler, *Science* **298**, 1381 (2002).
4. Y. Sugimoto et al., *Nat. Mater.* **4**, 156 (2005).
5. Y. Sugimoto et al., *Phys. Rev. Lett.* **98**, 106104 (2007).
6. M. Ternes, C. Lutz, C. Hirjibehedin, F. Giessibl, A. Heinrich, *Science* **319**, 1066 (2008).
7. O. Paz, I. Brihuega, J. M. Gómez-Rodríguez, J. M. Soler, *Phys. Rev. Lett.* **94**, 056103 (2005).
8. R. D. Piner, J. Zhu, F. Xu, S. Hong, C. A. Mirkin, *Science* **283**, 661 (1999).
9. Materials and methods are available as supporting online material on *Science* Online. In AFM experiments we used the easyPLL Plus (Nanosurf, Liestal, Switzerland) for the detection and regulation of the cantilever dynamics, and data acquisition and representation was performed using a Dulcinea SPM controller (Nanotec Electrónica, Madrid, Spain) (*29*).
10. T. R. Albrecht, P. Grütter, D. Horne, D. Rugar, *J. Appl. Phys.* **69**, 668 (1991).
11. S. T. Jemander, N. Lin, H. M. Zhang, R. I. G. Uhrberg, G. V. Hansson, *Surf. Sci.* **475**, 181 (2001).
12. Y. Sugimoto et al., *Phys. Rev. B* **73**, 205329 (2006).
13. M. A. Lantz et al., *Science* **291**, 2580 (2001).
14. Y. Sugimoto et al., *Nature* **446**, 64 (2007).
15. M. Abe, Y. Sugimoto, O. Custance, S. Morita, *Appl. Phys. Lett.* **87**, 173503 (2005).
16. N. Oyabu et al., *Phys. Rev. Lett.* **96**, 106101 (2006).
17. D. M. Eigler, C. P. Lutz, W. E. Rudger, *Nature* **352**, 600 (1991).
18. P. Jelinek, H. Wang, J. P. Lewis, O. F. Sankey, J. Ortega, *Phys. Rev. B* **71**, 235101 (2005).
19. F. J. Giessibl, *Phys. Rev. B* **56**, 16010 (1997).
20. J. E. Sader, S. P. Jarvis, *Appl. Phys. Lett.* **84**, 1801 (2004).
21. H. Hölscher et al., *Phys. Rev. B* **64**, 075402 (2001).
22. U. Dürig, *Appl. Phys. Lett.* **75**, 433 (1999).
23. N. Sasaki, M. Tsukada, *Jpn. J. Appl. Phys.* **39**, L1334 (2000).
24. L. N. Kantorovich, T. Trevethan, *Phys. Rev. Lett.* **93**, 236102 (2004).
25. G. Mills, H. Jónsson, *Phys. Rev. Lett.* **72**, 1124 (1994).
26. T. Shinada, S. Okamoto, T. Kobayashi, I. Ohdomari, *Nature* **437**, 1128 (2005).
27. B. E. Kane, *Nature* **393**, 133 (1998).
28. D. Kitchen, A. Richardella, J.-M. Tang, M. E. Flatté, A. Yazdani, *Nature* **442**, 436 (2006).
29. I. Horcas et al., *Rev. Sci. Instrum.* **78**, 013705 (2007).
30. S.Y., O.C., M.A., and S.M. acknowledge support from grants in aid for scientific research from the Ministry of Education, Culture, Sports, Science and Technology (MEXT), JST, Handai Frontier Research Center, the Project Atomic Technology funded by MEXT, and Global Center of Excellence program "Center for Electronic Devices Innovation." O.C. also acknowledges support from the Air Force Office of Scientific Research–Asian Office of Aerospace Research and Development. The work of Y.S. is supported by the Frontier Research Base for Global Young Researchers funded by MEXT. P.P. and R.P. acknowledge the support of Ministerio de Educación y Ciencia (Spain) and computer time provided by Red Española de Supercomputación at the Barcelona Supercomputing Center. P.J. acknowledges the support of Grantová Agentura Akademie Věd (Czech Republic)

Catalytic Conversion of Biomass to Monofunctional Hydrocarbons and Targeted Liquid-Fuel Classes

Edward L. Kunkes, Dante A. Simonetti, Ryan M. West, Juan Carlos Serrano-Ruiz, Christian A. Gärtner, James A. Dumesic*

It is imperative to develop more efficient processes for conversion of biomass to liquid fuels, such that the cost of these fuels would be competitive with the cost of fuels derived from petroleum. We report a catalytic approach for the conversion of carbohydrates to specific classes of hydrocarbons for use as liquid transportation fuels, based on the integration of several flow reactors operated in a cascade mode, where the effluent from the one reactor is simply fed to the next reactor. This approach can be tuned for production of branched hydrocarbons and aromatic compounds in gasoline, or longer-chain, less highly branched hydrocarbons in diesel and jet fuels. The liquid organic effluent from the first flow reactor contains monofunctional compounds, such as alcohols, ketones, carboxylic acids, and heterocycles, that can also be used to provide reactive intermediates for fine chemicals and polymers markets.

Diminishing petroleum reserves and growing concerns about global climate change necessitate the development of fuel production pathways based on renewable resources, such as biomass-derived carbohydrates. The conversion of biomass-derived carbohydrates to liquid transportation fuels requires removal of most, or all, of the oxygen atoms in the reactants to form molecules having desirable properties for combustion. To produce nonoxygenated liquid fuels, this removal of oxygen must be accompanied by isomerization to form branched hydrocarbons for gasoline, and/or by C-C coupling reactions to increase the molecular weight for diesel and jet fuels. We have previously outlined a strategy involving dehydration of sugars (e.g., fructose) over acid catalysts to form furan derivatives (e.g., hydroxymethylfurfural, HMF) that can subsequently undergo aldol condensation with ketones (e.g., acetone), followed by hydrodeoxygenation to form C_9 to C_{15} alkanes for use in diesel and jet fuels (*1, 2*). Here, we outline a strategy that begins the oxygen-removal process by converting sugars and polyols over a Pt-Re catalyst to form primarily hydrophobic alcohols, ketones, carboxylic acids, and heterocyclic compounds (Fig. 1). This process can be used to produce ketones for C-C coupling with HMF, thereby replacing the acetone in our previous process with ketones derived directly from biomass. This alternative process does not require the separate formation of HMF, because we demonstrate that the ketones produced can undergo self-coupling reactions. In addition, this process provides a route to highly branched alkanes and olefins, as well as alkylated aromatics, these compounds being high-octane components of gasoline (*3, 4*). Moreover, intermediate compounds formed during the conversion of biomass-derived carbohydrates to liquid transportation fuels can serve as valuable compounds for the chemical and polymer industries.

The conversion of carbohydrates over metal catalysts proceeds via reaction pathways involving C-C and C-O bond scission (*5, 6*). High rates of C-C cleavage lead to the formation of CO, CO_2, and H_2 (denoted as "reforming"), whereas high rates of C-O cleavage produce alkanes (*5, 6*). Our approach here is to achieve controlled rates of C-C and C-O cleavage, leading to the formation of monofunctional hydrocarbons. This behavior is analogous to achieving selective hydrogenation of acetylene to ethylene, without undergoing further reaction to form ethane over metal catalysts (*7*), where strongly adsorbed reactants preferentially occupy surface sites compared to more weakly adsorbed reaction intermediates, thus allowing the production of these reaction intermediates with high yield.

In the initial step of our process, a fraction of the polyol or sugar feed is reformed over Pt-Re/C to supply the hydrogen required to partially deoxygenate the remainder of the feed to monofunctional hydrocarbons. Endothermic reforming reactions are balanced with exothermic deoxygenation reactions in the same reactor, such that the overall conversion is mildly exothermic and more than 90% of the energy content of the polyol or sugar feed is retained in the reaction products. As outlined schematically in Fig. 1 for a polyol feed, we propose that reforming reactions involve adsorption and dehydrogenation of the polyol, followed by C-C cleavage, leading to CO adsorbed on the catalyst surface, which reacts with water to produce H_2 and CO_2 by the water–gas shift reaction. (This production of CO_2 is required for the overall conversion of polyols to monofunctional hydrocarbons, because a fraction of the polyol feed must be converted to H_2 and CO_2 to generate the hydrogen required for deoxygenation reactions.) Adsorbed polyol species

Department of Chemical and Biological Engineering, University of Wisconsin–Madison, Madison, WI 53706, USA.

*To whom correspondence should be addressed. E-mail: dumesic@engr.wisc.edu